Tikrit Journal of Engineering Sciences (2023) 30 (2): 46-59

DOI: http://doi.org/10.25130/tjes.30.2.6

IRAQI Academic Scientific Journals

ISSN: 1813-162X (Print); 2312-7589 (Online)

Tikrit Journal of Engineering Sciences

available online at: http://www.tj-es.com

TJES Tikrit Journal of Engineering Sciences

Design of New Composites Nano-Catalysts for Naphtha Reforming Process: Experiments and Process Modeling

Aysar T. Jarullah [a,c], Ahmed Nabeel Ahmed [a], Ban A. Altabbakh [b], Abdullah M. Ahmed [a]*

a Department of Chemical Engineering, College of Engineering, Tikrit University, Tikrit, Iraq.

b Petroleum Research and Development Center, Ministry of Oil, Baghdad, Iraq.

c School of Engineering, Design and Technology, University of Bradford, Bradford BD7 1DP, United Kingdom.

Keywords:

Molybdenum Carbide; Heavy Naphtha; Bimetallic Catalyst

ARTICLE INFO

Article history:

Received	11 Mar. 2023
Received in revised form	28 Mar. 2023
Accepted	02 May 2023
Final Proofreading	10 May 2023
Available online	14 May. 2023

Citation: Jarullah AT, Ahmed AN, Altabbakh BA, Ahmed AM. Design of New Composites Nano-Catalysts for Naphtha Reforming Process: Experiments and Process Modeling. *Tikrit Journal of Engineering Sciences* 2023; **30**(2): 46-59.
http://doi.org/10.25130/tjes.30.2.6

Corresponding author:

Aysar T. Jarullah

Department of Chemical Engineering, College of Engineering, Tikrit University, Tikrit, Iraq.

Abstract: The naphtha catalytic reforming process is evaluated by designing new composite nano-catalysts. Three catalysts were prepared for this process. The first catalyst was molybdenum carbide composite with platinum over HY zeolite (Mo_2C.Pt/HY zeolite), the second catalyst was molybdenum carbide composite with platinum over modified zeolite by cerium nitrate (Mo_2C.Pt/CeY zeolite), and the last catalyst was bimetallic titanium and platinum with a titanium content of 1% and platinum content of 0.11% over HY zeolite (Pt.Ti/HY zeolite). All catalysts were tested with several tests, mainly X-Ray Diffraction (XRD), BET surface area, and pore volume. All these substances were applied as catalysts for the reforming process of Iraqi heavy naphtha at the following operating conditions: reaction temperature (480, 500, and 520°C), reaction pressure (10, 12.5, and 15 bar), liquid hourly space velocity (LHSV) at 2 hr^{-1}, and constant hydrogen to hydrocarbon ratio (H_2/ HC) of 4. All the reforming reactions occurred in a packed bed pilot plant reactor to investigate its stability and activity during the reforming process. All the developed catalyst samples showed sensational stability even at operating under difficult circumstances. The best catalyst was Pt.Ti/HY zeolite based on the results obtained with respect to the octane number (86.2) at 520 °C and 15 bar. Also, a mathematical model to describe the reforming process with high accuracy was built and simulated using gPROMS software. The results were very satisfying since the most significant error with the wt% of reformate was 4.9% (the experimental aromatics content was 23.94 wt.%, while the predicted result was 21.67 wt.%), while Research Octane Number (RON) error was 4.7% (the experimental RON was 81, whereas the predicted value of RON was 85) among all the results meaning that the simulating was valid to describe the process.

تحضير مجموعة جديدة من العوامل المساعدة المركبة النانوية لعملية تهذيب النفثا: مختبريا وتصميميا رياضيا

ايسر طالب جارالله [1،3]، احمد نبيل احمد [1]، بان الطباخ [2]، عبدالله محمد احمد [1]
[1] قسم الهندسة الكيمياوية / كلية الهندسة / جامعة تكريت / تكريت - العراق. [2] مركز البحوث والتطوير النفطي / وزارة النفط / بغداد - العراق. 3 مدرسة الهندسة، التصميم والتكنولوجيا، جامعة برادفورد، برادفورد، المملكة المتحدة.

الخلاصة

تشمل هذه الدراسة على تحضير ثلاثة عوامل مساعدة نانوية مركبة لغرض تحسين عمليات تهذيب النفثا الثقيلة، العامل المساعد الأول هو المولبدينيوم كاربيد مركب مع البلاتين على الزيولايت،(Mo2.Pt/HY zeolite) العامل المساعد الثاني هو الموليبدينيوم كاربيد مركب مع البلاتين على الزيولايت المعدل بواسطة السيريوم(Mo2.Pt/CeY zeolite)، والعامل المساعد الثالث هو دالة ثنائية المعدن من التيتانيوم والبلاتين بنسب وزنية 0.11% بلاتين و 1% تيتانيوم على الزيولايت (Pt.Ti/HY zeolite). اجريت العديد من الفحوصات مثل حيود الاشعة السينية (XRD) والمساحة السطحية (BET) وحجم المسامة (Pore volume) والتي قد تم اخذها لكل العوامل المحضرة. تم استخدام جميع العوامل لغرض تقييم استخدامها لعمليات إعادة تشكيل النفثا الثقيلة العراقية عند الظروف التشغيلية التالية (درجات الحرارة (480, 500, 520 درجة مئوية)، وضغط (10, 12,5, و 15 بار) و معدل الهيدروجين الى الهيدروكاربون 6 مول/مول و سرعة السائل الفراغي 4 ساعة$^{-1}$) باستخدام مفاعل الطبقة الثابتة (packed bed reactor) لإعادة تشكيل النفثا الثقيلة. جميع العوامل المساعدة أظهرت ثباتية عالية في جميع الظروف التشغيلية المختلفة. اظهرت النتائج ان افضل عامل مساعد هو الثالث (Pt.Ti/HY zeolite) الذي قد انتج منتج بعدد اوكتاني 86,2 عند درجة حرارة 520 م وضغط 15 بار. أيضا، تم انشاء موديل رياضي باستخدام برنامج (gPROMS) وكانت نتائجه مرضية للغاية بنسبة خطأ تقدر ب 4,9% للنسب الوزنية للنواتج وكذلك 4,7% للعدد الاوكتاني ولجميع العوامل.

الكلمات الدالة: كربيد الموليبدينوم، النفثا الثقيلة، المحفز المعبئ.

1.INTRODUCTION

Catalytic reforming is considered the refining process that is evolving fast, and numerous studies that have been done on its various aspects, with a particular emphasis on three crucial issues: researching and developing new catalysts with improved activity, selectivity, and deactivation; examining the reforming reaction and disclosing appropriate kinetics as well as deactivation models; and presenting or providing reactor configuration and operation type with improved deactivation. Metal and oxide components are active parts in commercial catalysts, which typically utilize platinum metal distributed over porous promoted alumina or silica-alumina bases [1-3]. Numerous possible uses for zeolite with mesoporosity and microporosity include enhanced catalytic activity and stability in numerous catalytic processes [4]. The reforming of naphtha typically uses platinum catalysts, which due to coke formation's fast deactivation, high-pressure procedures, and bimetallic catalysts, are utilized to satisfy the ever-stricker specifications. Tin, rhenium, or iridium are examples of metallic materials [5]. Hydrogenation and dehydrogenation reactions are performed on the metallic site of the bi-functional catalyst used in catalytic reforming activities, whereas isomerization, cracking, and cyclization reactions are conducted on the acidic site. The catalyst should possess strong acidic qualities since it must be able to transform the naphtha feed into more advantageous products. The crystalline aluminosilicate (zeolite), which has certain qualities, including ion-exchange ability, high exchange capability, crystalline structure with regular pores, and precise silica-to-alumina ratio, is another advantage of the platinum catalyst. The bi or multi-metallic compounds are typically supplied to the zeolite pores and decrease it to their ionic state with hydrogen that favors aromatic hydrocarbons, so the metal is mainly presented atomically in the zeolite lattice pores [6]. Another type of catalyst was recently introduced, i.e., transition metal carbide (TMC). These carbide materials display unusual blended covalent solids, ionic crystals, and transition metal characteristics. These substances have high melting points and electrical characteristics comparable to ionic solids, are tougher than covalent solids, and are thermally stable, like transition metals [7]. TMC materials like molybdenum and tungsten carbides have been successfully used as catalysts for isomerization and dehydrogenation reactions, essential metal-based reactions in naphtha reforming. However, unlike the noble metal Pt supported by alumina is employed unsupported, which may explain why the catalyst performance is not similar to that of Pt. Even though the materials have the same electrical structure as Pt, they also need the right surface area, dispersion, and access to the catalyst's active site to react effectively [8]. The four primary reactions in the catalytic reforming process are naphthenes dehydrogenation, isomerization of paraffin and naphthenes, dehydrocyclization of paraffin, and hydrocracking and dealkylation. In the catalytic reforming of petroleum naphtha, an average of 50 to 200 cubic meters of hydrogen (at zero degrees Celsius) and one atmospheric pressure are produced for every

cubic meter of liquid naphtha feedstock [9]. This hydrogen can be used in refinery plants, such as hydrodesulfurization [10]. Typically, naphtha reforming units are categorized by the method used for catalyst regeneration: cyclic catalytic reformer, semi-regenerative catalyst reformer, and continuous catalyst regeneration reformer are examples of catalyst reformers (CCR) [11]. The majority of prior research works were presented with reforming in batch reactors utilizing pure synthetic fuel [12]. The present study introduced transition metal carbide with platinum over HY zeolite to the catalytic reforming reactions of heavy naphtha inside a packed bed reactor. Also, the performance of commercial HY zeolite (with Pt–Ti loading) was investigated in more detail. As well as the modified Y zeolite with transition metal carbide (molybdenum carbide) and Pt performance was designed and studied in the same pilot plant. A mathematical model for the reforming process for all the prepared catalysts has been built via gPROMS software to describe the process and compare the results predicted with experimental results generated from the pilot plant.

2. EXPERIMENTAL SECTION

2.1. Feed Stock

Heavy Naphtha supplied by the North Refineries Company/ Baiji as raw material for the reforming activity test was used. Some properties of heavy naphtha given by the supplier are listed in Table 1. All the materials used to prepare the catalysts are shown in Table 2.

Table 1 Properties of Heavy Naphtha Properties.

Properties	
Sulfur content, ppm	0.1%
Density, g /cm³	0.73
Paraffins, wt.%	61.3
Aromatics, wt.%	13
Naphthenes, wt.%	25.7
I.B.P, °C	40
E.B.P, °C	280
RON	57

Table 2 The Chemical Compounds Used in This Study.

Chemicals	Formula, %	Molecular weight g/gmol	Purity	Supplier
Activated carbon	C	14	100	
HY-zeolite			99	Alfa Nanomaterials Chemistry
Ammonium Molybdate tetrahydrate	$(NH_4)6Mo_7O_{24}.4H_2O$	115.03	99	ROMIL
Hexachloroplatinic acid	$H2PtC_{16}.6H_2O$	517.92	40	REIDL
Cerium nitrate	$CeN_3O_9.6H_2O$	434.22	99	SIGMA - ALDRICH
Titanium Butoxide	$Ti(OCH_3)$	340.32	97	SIGMA - ALDRICH

Three samples of catalysts were synthesized. The first was molybdenum carbide with platinum over HY zeolite Mo2C.Pt/HY, the second was molybdenum carbide with platinum over modified Y zeolite by cerium Mo2C.Pt/CeY zeolite, and the third one was a bimetallic catalyst with 0.11% Pt and 1% Ti over HY zeolite.

2.2.Experimental Procedure

2.2.1. Mo2C.Pt/HY zeolite preparation

Molybdenum carbide was produced via solid-state synthesis and supported on carbon. It is a conventional technique that involves adding activated carbon to the metal salt solution and stirring it for two hours at 130 °C. After that, the solvent was evaporated, and the mixture was dried for four hours in a 150 °C oven. The carbon and metal precursors were calcinated at three distinct temperatures of 800, 900, and 1000 °C at a ramp rate of 4.5 °C/h under nitrogen flow, and they were allowed to remain at those temperatures for two hours. After the reaction, the catalyst was cooled to room temperature. 175 ml of cold water was diluted with 0.43 g of hexachloroplatinic acid at room temperature. Then, 70 g of HY-Zeolite was added, and the mixture was agitated for 30 minutes without heating. The mixture was then left to settle overnight. The solution was filtered, cleaned, and put into a dryer to remove all water after one day. The resulting white powder was decreased and then calcined at 260°C for three hours. Platin makes up 0.25 percent of HY-Zeolite. The prepared molybdenum carbide with the prepared Pt/HY zeolite was mixed with 7 wt.% PVA, 23 wt.% Kaoline, and an appropriate amount of water to form a paste, which was put in the granulator and then dried overnight at 110 °C and calcined at 400 °C for 2 hours at a rate of 2 °C/ min. The dried extrudates were cut into pieces, i.e., 3–7 mm long. The calcinated catalyst was then reduced with hydrogen at 350 °C for 3 hours [8].

2.2.2.Mo2C.Pt/CeY zeolite preparation

Ion exchange using nitrate solutions of the cerium cation Ce(NO3)3 at a certain concentration of the zeolite HY powder was designed. A Ce-modified zeolite Y was created by ion exchanging the sample at 80 °C for 8 hours in accordance with the previously indicated ratio of 50 g Zeolite HY to 600 mL nitrate solution, followed by filtering, washing, drying at 120 °C for 8 hours, and calcining at 600 °C for 5 hours. In the separate funnel, 0.14 grams of hexachloroplatinic acid was dissolved in distilled water. After the powder was calcined, it was charched into a flask, vacuumed the air before adding the solution gently, mixed it thoroughly, and let sit until the following day. Then the material was cleaned, filtered, and dried before entering the furnace for six hours at 600°C. Then, the Pt/CeY zeolite was mixed with molybdenum carbide and 7 wt.% PVA, 23 wt.% Kaoline, and the rest procedure was the same procedure mentioned above [1].

2.2.3.Pt.Ti/ HY zeolite

By co-impregnation technique, 100 g of obtained HY-zeolite powder was used to

manufacture 0.11 weight percent Pt and various weight percent of Ti (1 wt%). Chloroplatinic acid solution and the appropriate titanium butoxide solution were first prepared. The HY zeolite was then placed in a vacuum, and the solution was added drop by drop while stirred magnetically. Then the vacuum was turned off, and the sample was mixed for two hours to achieve a uniform distribution of metal precursors. The slurry was then filtered, cleaned with distilled water, dried at 110°C overnight, and then calcined for three hours at 260°C at a rate of 2°C/min [13].

2.3. Catalyst Performance

The synthesized catalyst was tested in a fixed-bed reactor to determine its efficacy. In order to provide a smooth flow and enough surface area for the reaction to occur, the catalyst was first deposited in the fixed bed between two inert ceramic balls. When the temperature reached the desired level, the hydrogen valve was opened to remove air from the system before turning on the heavy naphtha dosing pump. Before the reactor, hydrogen and heavy naphtha were pre-mixed, and the reaction started on the catalyst when the combination entered the reactor. The product was cooled down using a cooler, and the hydrogen was removed from the system using a high-pressure. The reformate products were analyzed using Gas Chromatography Analyzer (GC). Fig. 1 shows a picture of a pilot plant for heavy naphtha reforming.

Fig.1 Image of the Heavy Naphtha Reforming Unit (Pilot Plane).

2.4.Catalyst Activity

In the reforming pilot unit, samples of the produced Mo2C.Pt/HY zeolite, Mo2C.Pt/CeY zeolite, and Pt-Ti/HY zeolite were tested for their catalytic activity using a fixed bed carbon steel reactor with a 2.5 cm diameter under a whole control process with cooling equipment that made up the apparatus. The reactor was filled with 60 g of the prepared catalyst substance for each experiment. The top and bottom halves of the fixed bed reactor were stuffed with ceramic balls (5–6 mm). Investigations were conducted at three reaction temperatures of 480, 500, and 520 °C at working pressures of 10, 12.5, and 15 bar, with H2/HC ratios of 4 and 2 hr-1 LHSV. Before the test, the catalyst was degraded with hydrogen gas at 450°C for three hours. The reaction occurred when heavy naphtha was pushed through a catalyst bed and combined with hydrogen. The product obtained was cooled with a cooling system, then separated by a separator to create "reformate" that was then collected and subjected to GC analysis (Type, 3300 Varian) to check the paraffin (iso-paraffin and n-paraffin), aromatics, and naphthenes content. The research octane number, or "RON," was also calculated using a suitable octane number analyzer. Fig. 2 shows a schematic diagram of the pilot plant system.

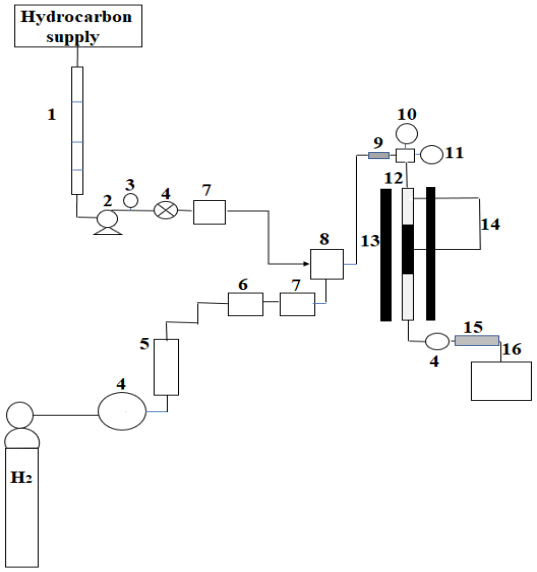

1- Metering burette
2- Dosing pump
3- Liquid flow meter
4- Needle valve
5- H_2 flow meter
6- 5A – Molecular sieve dryer
7- One-way valve
8- Mixing section
9- Feed preheating zone
10- Temperature controller system
11- Pressure controller system
12- Stainless steel reactor
13- Heating furnace
14- Thermocouples system
15- Cooling system
16- Gas chromatography

Fig.2 A schematic Diagram of the Pilot Plant System.

3. RESULTS AND DISCUSSIONS:

3.1. Catalyst Evaluation

X-ray diffraction, BET surface area, and pore volume were analyzed for all catalysts to evaluate it. The physical and chemical properties of prepared catalysts are tabulated in Table 3.

Table 3 Physical and Chemical Properties of Catalysts.

Catalysts	Surface area (m^2/g)	Pore volume (cm^3/g)	Bulk density (g/cm^3)	Crushing strength (kg)
Mo_2C.Pt/HY	724.55	0.75	0.468	1.89
Mo_2C.Pt/CeY	734.55	0.64	0.567	1.66
Pt.Ti/ HY	575	0.381	0.601	1.83

3.1.1.X-Ray Diffraction Analysis

The XRD pattern diffractogram of the prepared molybdenum carbide and all catalysts are shown in Fig.2. The X-ray diffraction analysis for molybdenum carbide is shown in Fig.3 (a). There are carbon index peaks at 2 θ = 20.549, 31.89, and 42.827 showing a high level of crystallization for the band of 2θ from 0^o to 45^o; this result is in agreement with Hodala et al. [8]. The X-Ray diffractogram of the Mo2C.Pt/HY zeolite catalyst is illustrated in Fig. 3 (b), giving a high level of crystallization for the band from 0^o to 35^o. There are zeolite index peaks at 2 θ = 11.8, 15.7, 20.5, 23.6, 27, 32.4, and 43.1. For the Mo2C.Pt/CeY zeolite, the X-ray diffractogram is displayed in Fig.3 (c), and the zeolite indexed peaks are noted in 2θ =10.33, 12.18, 15.9, 18.9, 20.55, 23.04, 27.3, 31.7, and 38.2 showing a high level of crystallization for the band of 2θ from 10° to 40°. While Fig.3 (d) shows Pt.Ti/HY zeolite X-ray diffractogram.

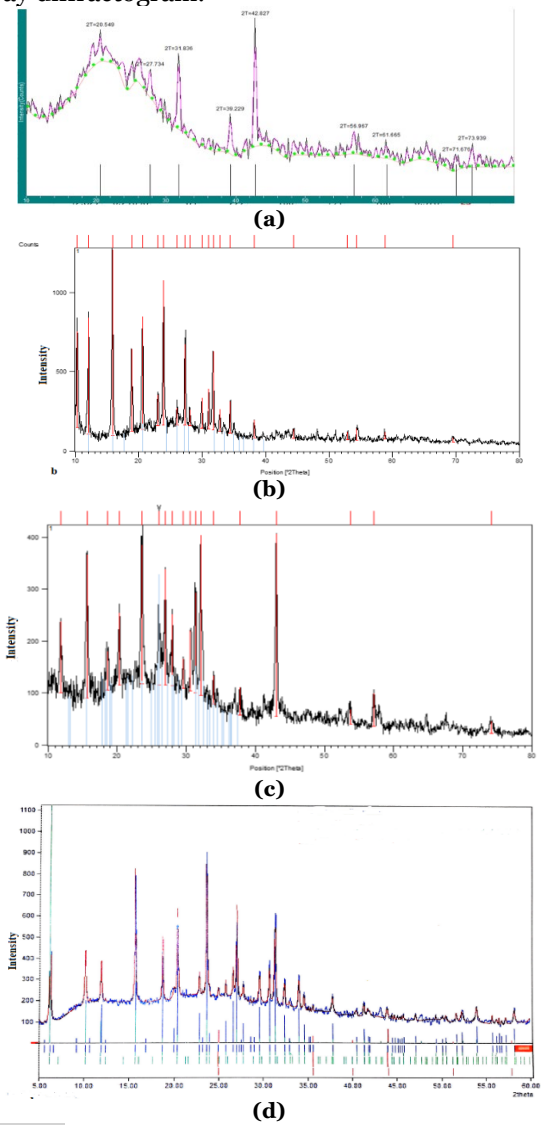

Fig.3 X-Ray Diffraction for all Substances **(a)** Molybdenum Carbide, **(b)** Mo_2C.Pt/HY Zeolite, **(c)** Mo_2C.Pt/CeY Zeolite, and **(d)** PT.Ti/HY Zeolite.

The zeolite's structure was unchanged by the ion exchange, showing a high crystallization for the band from 0° to 33°. Using Scherer's equation (1) below, the crystal size L is determined as follows [14]:

$$\beta(2\theta) = \frac{K\lambda}{L\cos\theta} \quad \textbf{(1)}$$

where K is the Scherrer's constant, which can be ranged from 0.6 to 2.08 depending on the crystal form; (for convenience, it has been assumed to be 1 here); β is the line broadening in radians (FWHM) of the peak at 2θ; and λ is the center frequency of the spectrum. The X-ray diffractometer uses radiation with a wavelength of (Cu K α, 1.5406). The crystal size of all prepared catalysts calculated from Scherrer's equation is illustrated in Table 4.

Table 4 Scherrer Equation Crystal Size for all Catalysts.

Catalyst	Crystal size (nm)
Mo_2C	18.65
Mo_2C.Pt/HY zeolite	20.77
Mo_2C.Pt/CeY zeolite	40.43
PT.Ti/HY zeolite	25.77

3.1.2(BET) Surface Area and Pore Volume Analysis

Table 5 shows the prepared molybdenum carbide and all catalysts' specifications. The surface area and pore volume were tested at the Iraqi Ministry of Oil's/Petroleum Research and Development Center (PRDC)-Baghdad. All the synthesis catalysts had a large surface area, indicating that larger voids among the particles increased the catalyst's pore volume. Hence, due to its enormous surface area, the produced catalyst may function as a highly chemically active catalyst for the heavy naphtha reforming process

Table 5 BET Surface Area and Pore Volume for all Prepared Catalysts.

Catalyst	BET surface area m^2/g	Pore volume cm^3/g
Molybdenum carbide	1072	-
Mo_2C.Pt/HY zeolite	724.55	0.778
Mo_2C.Pt/CeY zeolite	734.55	0.682
Pt.Ti/HY zeolite	575	0.381

4. CATALYSTS' PERFORMANCE

4.1 Effect of Operating Conditions on Catalytic Reforming

It is clear that by employing all catalyst samples to several degrees at the whole range of temperature investigated, the RON of the feed of heavy naphtha was increased. At the operating conditions of 15 bar and 520 °C, the greatest rise of octane number was 29 units. The research results are provided in Figs. (3-5). The octane number, which measures the quality of the generated reformate, varied from 70.8 to 86.2. The catalyst sample of Pt.Ti/HY zeolite produced the highest octane number (86.2), which can be explained by the acidic catalyst's metallic action. The dehydro-cyclization of paraffin and the dehydrogenation of naphthenes rose with this loading, increasing

the aromatic contents and, in turn, the reformate's octane number [15]. The results of Mo2C.Pt/HY zeolite showed a good result at 500 °C and 15 bar, while the Mo2C.Pt/CeY zeolite achieved the maximum octane number, i.e., 78.2, at 500 °C and 15 bar.

Splitting big molecules like n-decane into C3 and C7 to increase octane allows the latter to undergo an aromatization process to become fragrant. It may be concluded from a comparison of the action under the current operating pressure (10 bar, 12.5 bar, and 15 bar) that utilizing the highest pressure (15 bar), the octane number reached 86, higher than the previous reading by two points. However, increasing the working pressure in the current work at 10 bars caused a rise of hydro-cracking reactions [16], which reduced the yield of the generated reformate but lowered the coke formation on the catalyst, saving the catalyst from sintering. Figs. (4- 6) show the octane numbers for all catalysts at all operating conditions of the present study.

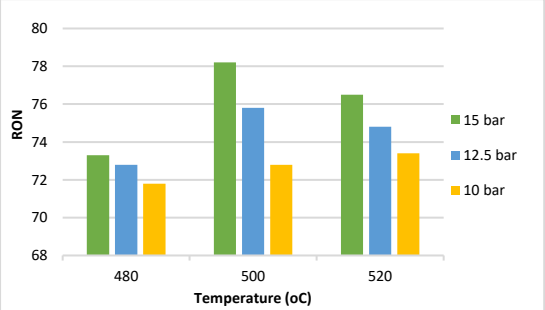

Fig.4 Octane Number Versus Reaction Temperature for Mo2C.Pt/HY Zeolite.

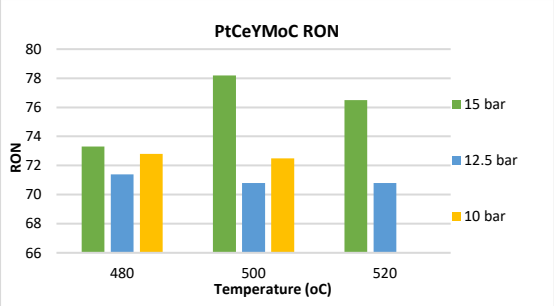

Fig.5 Octane Number Versus Reaction Temperature for Mo2C.Pt/CeY Zeolite.

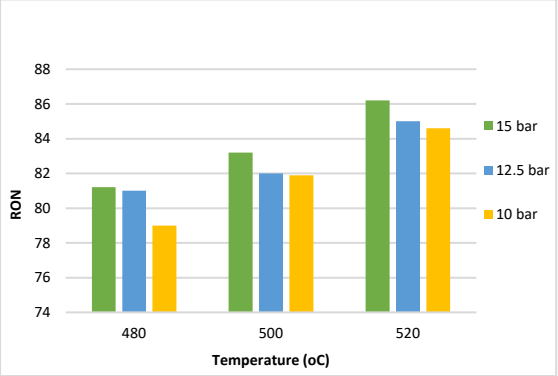

Fig.6 Octane Number Versus Reaction Temperature for Pt.Ti/HY Zeolite.

4.2.Catalyst performance and reformate yield

In general, a catalyst's activity refers to how well it performs with the reaction rate, which means when the reaction rate is high, the content of the desired product is significant, more particularly, the higher product of aromatic during catalytic reforming. The metal loading affects the support's acidic characteristics, affecting the produced catalysts' activity and selectivity. The ratio of product reformate to heavy naphtha feed is called the reformate yield. The overall yield of reformate is highly correlated with the total amount of naphtha converted, and when reformate quality improves, the yield declines and vice versa. All product compositions are shown in Tables (6-8) for all catalysts. For the first catalyst (Mo2C.Pt/HY zeolite), the highest quantity of aromatics obtained at 520 °C and 15 bar was 26.57 wt%, and the lowest quantity at 480 °C and 10 bar was 19.9 wt%. For Mo2C.Pt/CeY zeolite, the highest quantity was 26.56 wt% at 500 °C and 15 bar, and the lowest was 20.66 wt% at 520 °C and 12.5 bar. While for Pt.Ti/HY zeolite, the highest aromatics wt% was 27.2 at 520 °C and 15 bar, and the lowest composition of aromatics was 22.8 wt%. From the results obtained for all catalysts, changing the operating conditions was important in aromatics formation. The temperature can affect the reactions that lead to aromatics formation giving a high research octane number. Regarding this study, the best results were obtained by Pt.Ti/HY zeolite due to the bimetallic function of titanium at 1% with platin at 0.11%. When the temperature and pressure were raised, the aromatic content in the product increased due to naphthenes dehydrogenation.

Table 6 Product Composition for Mo2C.Pt/HY Zeolite.

Reaction temperature (°C)	Reaction pressure (bar)	Parafins (wt.%)	Naphthene (wt.%)	Aromatics (wt.%)
480	15	63.9	12.72	23.38
480	12.5	64.02	12.08	23.9
480	10	64.76	15.34	19.9
500	15	60.3	15.3	24.4
500	12.5	62.53	13.11	24.36
500	10	63.71	12.35	23.94
520	15	62	12.17	25.83
520	12.5	62.66	14.41	22.93
520	10	60.58	12.85	26.57

Table 7 Product Composition for Mo2C.Pt/CeY Zeolite.

Reaction temperature (°C)	Reaction pressure (bar)	Parafins (wt.%)	Naphthene (wt.%)	Aromatics (wt.%)
480	15	60.74	13.67	25.59
480	12.5	61.52	12.04	26.44
480	10	63.16	13.03	23.81
500	15	60.42	13.02	26.56
500	12.5	64.74	11.95	23.31
500	10	61.43	13.91	24.66
520	15	64.93	10.11	24.96
520	12.5	66.98	12.36	20.66
520	10	61.85	13.58	24.57

Table 8 Product Composition for Pt.Ti/HY Zeolite.

Reaction temperature (°C)	Reaction pressure (bar)	Paraffins (wt.%)	Naphthene (wt.%)	Aromatics (wt.%)
480	15	60.4	12.2	26.4
480	12.5	60.3	13.3	25.4
480	10	60.4	13.8	25.8
500	15	61.9	11.4	26.7
500	12.5	64.5	12.1	23.4
500	10	65.3	11.9	22.8
520	15	63.5	9.34	27.2
520	12.5	62.3	12.5	25.5
520	10	64	12.3	23.7

5. Description of the Reactor Models

When creating a generalized reactor model, nothing should be ignored a priori; however, all resistances and other variables must be accounted for in the mass and heat balance equations. Even if all the relevant parameters are accessible, such a model might still be complex and challenging to solve, necessitating some assumptions. Of course, the hypotheses must be solidly backed up by evidence, ideally experimental data. The generalized reactor model for processing is described, along with the detailed mass and heat balance equations that were created under the following presumptions: The characteristics of the liquids and gases (such as their surface velocities, mass and heat dispersion coefficients, specific heats, holdups, and densities), the catalysts (such as their porosity, size, activity, and effectiveness), the wetting efficiency, and the bed void fraction are all constant throughout the catalyst bed.

Here, the mathematical models for the reforming process were developed based on the following presumptions:

- The experimental device was operating in a steady state.
- The reactor was an isotherm.
- The gaseous reactant was in significant excess, and the liquid was constantly saturated with gas.

The necessary information, tools, and assumptions for simulation and modeling processes of heavy naphtha catalytic reforming are shown in Fig.7.

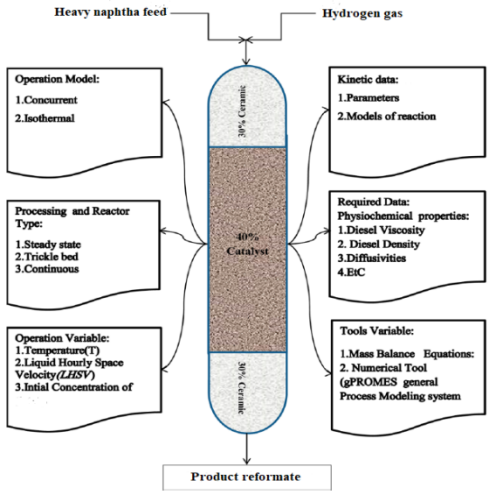

Fig. 7 Fixed Bed Reactor.

5.1 Models Based on the Kinetics

Numerous investigators have shown that the pore diffusion effects may be considered. Inside the confines of an apparent or effective response speed constant, or multiplying inherent to create a simple plug flow model with a pseudo-homogeneous behavior, multiply the reaction rate constant by the effectiveness factor, which helps outline how chemical reactions proceed.

For every molecule entering the reactor, the overall mass balance over the catalytic reactor is

[input] = [output] + [generation by reaction] + [accumulation] **(2)**

Since, $F_i = C_i v_L$

$$F_i = (F_i + dF_i) + (-r_i)dV \quad \textbf{(3)}$$

The equation that accounts for (i) is obtained after variable separation and the introduction of the space-velocity notion (LHSV $=v_L/V$). The compound is labeled in the differential part of the catalyst as

$$\tau = C_i \int_0^{X_i} \frac{dX_i}{-r_i} \quad \textbf{(4)}$$

where $-r_i$ is influenced by the material's concentration or conversion.

Assuming nth-order kinetics makes it reasonable to assess the reaction's chemical complexity. $(-r_i = K_{app} C_i^n)$. The intrinsic kinetics and apparent kinetics can be connected. Internal diffusion and the hydrodynamic effects are as follows:

$$\mathrm{k_{app}} = \eta_0 \eta_{ce} k_{in} \quad \textbf{(5)}$$

where η_0 is the catalyst effectiveness factor, and η_{ce} is the external catalyst wetting efficiency. The chemical reaction rate is calculated from

$$-r_i = \eta_0 \eta_{ce} k_{in} c_i^n \quad \textbf{(6)}$$

When the Arrhenius equation is used in this equation, the reaction rate becomes

$$-r_i = \eta_0 \eta_{ce} k_0 e^{\frac{-EA}{RT}} c_i^n \quad \textbf{(7)}$$

After integration:

$$\frac{1}{n-1}\left[\frac{1}{C_{jf}^{n-1}} - \frac{1}{C_{j0}^{n-1}}\right] = \frac{K_{app}}{LHSV} \quad \textbf{(8)}$$

Dudukovic [17] suggested that the liquid-phase reactant-limited processes. Thiele modulus for nonvolatile liquid reactants is a function of the catalyst effectiveness factor and partial surface-wetting effects coupled with local phenomena in the reactor, considering both fractional pore fill-up and insufficient external wetting (or internal partial wetting). The structure of a catalyst's pore and the physical characteristics (especially surface tensions) of the interacting gas, liquid, and solid systems determine the fractional pore fill-up. The volumetric average of the reaction rate inside the particle divided by the reaction rate at the particle's surface is referred to as the effectiveness factor of independent reactions, according to:

$$\eta_0 = \frac{\tanh \varphi_i}{\varphi_i} \quad \textbf{(9)}$$

The generalized Thiele modulus (φ_i) for the nth-order irreversible reaction is

$$\varphi = \frac{V_P}{S_P}\sqrt{\left(\frac{n+1}{2}\right)\left(\frac{r_j C_i^{-1}\rho_p}{D_{e,i}}\right)} \quad \textbf{(10)}$$

The pore network's structure (porosity and tortuosity) inside the particle is considered in the modeling by the effective diffusivity (D_{ei}).

$$D_{e,i} = \frac{\epsilon_S}{\tau}\frac{1}{\frac{1}{D_{mi}}+\frac{1}{D_{ki}}} \quad \textbf{(11)}$$

where (ϵ_S) can be calculated using the following equations:

$$\epsilon_S = \rho_p V_g \quad \textbf{(12)}$$

$$\rho_p = \frac{\rho_p}{1-\epsilon_B} \quad \textbf{(13)}$$

where ($\rho_p V_g$) is the catalyst porosity, and Vg is the total pore volume.Knudsen diffusivity D_{ki} and molecular diffusivity D_{mi} are two diffusion components that make up the effective diffusivity inside the catalyst particle. The Knudsen diffusivity factor (D_{ki}) and molecular diffusivity D_{mi} are calculated from [13, 14, 18].

$$D_{mi} = 8.93\ x\ 10^{-8}\frac{v_L^{0.267}T}{v_i^{0.433}\mu_L} \quad \textbf{(14)}$$

$$D_{ki} = 9700 r_g \left(\frac{T}{MW_i}\right)^{0.5} \quad \textbf{(15)}$$

where T is the temperature in K, and r_g is the mean pore radius that can be calculated by the following equation [19, 20]:

$$r_g = \frac{2V_g}{S_g} \quad \textbf{(16)}$$

A Riazi–Daubert correlation is used to determine the oil feedstock molar volume (vi) and critical specific volume (v_{cL})[21, 22].

$$v_L = 0.285\ (v_{cL})^{1.048} \quad \textbf{(17)}$$

v_{cL} is HN Critical volume

$$v_{cL} = (7.5214\ X\ 10^{-3}(T_{meABP})^{0.2897} (\rho_{15.6})^{-0.7666})MW_L \quad \textbf{(18)}$$

Because the pores in the catalysts are not aligned along the normal path from the surface to the pore of the catalyst particle, the pore network's tortuosity factor ($\mathcal{T}$) is considered while calculating D_{ei} [18].

$$\frac{1}{\mathcal{T}} = \frac{\epsilon_S}{1-\frac{1}{2}\log\epsilon_S} \quad \textbf{(19)}$$

At the atmospheric pressure, the external catalyst surface η_{ce} may be calculated with the Al-Dahhan and Dudukovic correlation [23].

$$\eta_{CE} = 1.104\ Re_L^{\frac{1}{3}}\left\{\frac{1+\left[\frac{\frac{\Delta P}{Z}}{\rho_L g}\right]}{Ga_L}\right\} \quad \textbf{(20)}$$

Reynolds number

$$Re_L = \frac{\rho_L u_L d_P}{\mu_L} \quad \textbf{(21)}$$

Modified Reynolds number

$$Re_L'' = \frac{\rho_L u_L d_P}{\mu_L(1-\epsilon_S)} \quad \textbf{(22)}$$

Galileo number

$$Ga_L = \frac{\rho_L g d_P}{\mu_L^2} \quad \textbf{(23)}$$

Modified Galileo number:

$$Ga_L'' = \frac{\rho_L^2 g d_P^3 \epsilon_B^3}{\mu_L^2(1-\epsilon_B)^3} \quad \textbf{(24)}$$

For an undiluted catalyst bed, bed void fraction (or bed porosity) may be calculated as follows [23]:

$$\epsilon_B = 0.38 + 0.073\left(1 + \frac{\left(\frac{d_t}{d_{pe}}-2\right)^2}{\left(\frac{d_t}{d_{pe}}\right)^2}\right) \quad \textbf{(25)}$$

The external volume and external surface of the catalyst can be estimated according to the particle's shape

Assuming a cylindrical shape

$$V_p = \pi r^2 h \quad \textbf{(26)}$$

$$S_p = 2\pi r h \quad \textbf{(27)}$$

The Standing Katz equation determines the oil density (ρ_L) as a function of temperature and pressure [24]:

$$\rho_L = \rho_o + \Delta\rho_p - \Delta\rho_T \quad \textbf{(28)}$$

Pressure depended on liquid density is represented by the following equation:

$$\Delta\rho_p = (0.167 + 16.181\ x\ 1^{-0.0425\rho_o}).\left(\frac{P}{1000}\right) - 0.01\ x\ (0.299 + 263\ x\ 10^{-0.0603\rho_o}).\left(\frac{P}{1000}\right)^2 \quad \textbf{(29)}$$

Glaso's equation has been used as a generalized mathematical equation for oil viscosity. The equation has the following form [25, 26]

$$\mu_L = 3.141\ x\ 10^{10}(T-460)^{-3.444}[\log API]^a \quad \textbf{(30)}$$

API is American Petroleum Institute, T is the temperature in K, a is a dimensionless number

$$a = 10.313[\log(T-460)] - 36.447 \quad \textbf{(31)}$$

$$API = \frac{141.5}{Sp.gr_{15.6}} - 131.5 \quad \textbf{(32)}$$

$$RON = 31.0621 + 0.53542 * T \quad \textbf{(33)}$$

where T is the boiling point in ºC for the individual component [27, 28].

Then the reformate octane number is calculated using the following equation:

$$RON = X_P^*(RON)_P + X_N^*(RON)_N + X_A^*(RON)_A \quad \textbf{(34)}$$

The reforming process model (Eqs. 2–34) was applied and solved by gPROMS software.

5.2.Estimation of Model Parameters

Several system parameters and chemical characteristics must be estimated to solve the set of ordinary differential equations (ODEs) for the steady-state regime or the set of partial

differential equations (PDEs) for the dynamic domain. These characteristics may be assessed using known correlations, whose precision is crucial for the reactor model's overall robustness. Some factors that affect bed characterization include others that are experimental or can be measured experimentally, whereas others can only be discovered empirically. Thus, even while experimentally determining the local porosity is preferred for measurements requiring sophisticated methods that might be costly. As a result, computational computations are frequently favored. For parameter calculation, the objective function, *OBJ*, as given below, is minimized:

$$OBJ = \sum_{n=1}^{Nt}\left(C_j^{meas} - C_j^{pred}\right)^2 \quad \textbf{(35)}$$

where Nt is the test runs numbers, $C_j^{meas}$is the measured concentration, and C_j^{pred} is the predicted concentration by the model. The first stage in the computation used kinetic parameters given using the gPROMS-created process model to evaluate the composition of all fractions in the literature. The next step in the below-mentioned optimization challenge was to update the kinetic parameters by reducing OBJ. The gPROMS software offers modern parameter estimation tools, including thorough statistical analysis employing data from nonlinear process models. Table 9 shows the magnitude of specified variables and constant parameters that are fixed in the model.

Table 9 Values of the Constant Parameters Used in the HN Reforming Models.

Parameter	Symbol	Unit	Value
Temperature	T1, T2, T3	K	T1= 753.15, T2= 773.15, T3= 793.15
Pressure	P	bar	P1 = 10 P2 = 12.5 P3 = 15
Liquid hour space velocity	LHSV1,	hr^{-1}	LHSV= 2
Initial concentration	C_o	wt.%	C1=0.2856, C2= 0.326, C3= 0.1557, C4= 0.231
Naphtha's density at 15.6 °C and 101.3 kPa	Den	g/cm^3	0.702
Gas constant	R	J/mole. K	8.314
Catalyst particle volume	V_p	cm^3	CAT1=1.794E-20 CAT2= 1.88E-18 CAT3=1.09E-16
Total external area of geometric of particle	S_p	cm^2	CAT1=3.3141E-13 CAT2=2.7E-9 CAT3=2.2E-8
Bulk density	bulk	g/cm^3	CAT1=0.468 CAT2=0.567 CAT3=0.575
Pore volume per unit mass of catalyst,	V_g	cm^3/g	CAT1=0.778 CAT2= 0.682 CAT3= 0.381
Molecular weight of gas	M_{wt}	g/gmole	2
Molecular weight of Naphtha	M_{wtL}	g/gmole	198
Critical specific volume	V_C	cm^3/mole	315.4
Mean average boiling point	T_{MeABP}	K	668.07
Particle specific surface area	S_g	cm^2/g	2597540
Tube diameter	d_t	cm	2
Velocity	u	cm/sec	u= 12.3
Acceleration gravity	g	cm/sec^2	981

The two steps that make up the gPROMS optimization solution are as follows: firstly, it drove a simulation to meet the (inequality constraints) and to converge all of the equality criteria. Secondly, it optimized (updates the magnitude of the decision variables, such as the kinetic parameters).

5.3.Estimation of Kinetic Parameters.

The kinetic parameters for the heavy naphtha reforming process presented in this work were estimated utilizing the experimental data from the fixed bed reactor. The composition of all products was determined by applying model equations in gPROMS using the kinetic parameters cited in the literature as a starting approximation. The optimization approach was used to minimize this variance in the model parameters. The calculated kinetic parameters for the catalytic reforming process are shown in Tables (10-12) for all catalysts. These Tables showed a significant difference between expected and experimental values. The reaction order and reaction constants are different for each catalyst. The software calculated its optimal values that can describe the process. For the Mo_2C.Pt/HY zeolite, the reaction order was 1.43893, and for Mo_2C.Pt/CeY zeolite, the reaction order was 1.6552, while for Pt.Ti/HY zeolite, the reaction order was 1.33293. The optimal reaction specification is the most crucial parameter in describing the system because it can describe all the process results.

Table 10 The Optimal Model Parameters for Mo_2C.Pt/HY.

Parameter	Value	Units
N	1.43893	(--)
k_1	0.49906	$hr^{-1}(wt.\%)^{-0.43893}$
k_2	1.036	$hr^{-1}(wt.\%)^{-0.43893}$
k_3	2.48282	$hr^{-1}(wt.\%)^{-0.43893}$

Table 11 The Optimal Model Parameters via Optimization Process for Mo_2C.Pt/CeY.

Parameter	Value	Units
N	1.6552	(--)
k_1	0.3972	$hr^{-1}(wt.\%)^{-0.6552}$
k_2	1.002	$hr^{-1}(wt.\%)^{-0.6552}$
k_3	2.2247	$hr^{-1}(wt.\%)^{-0.6552}$

Table 12 Optimal Model Parameters via Optimization Process for Pt.Ti/HY.

Parameter	Value	Units
n	1.33293	(--)
k_1	0.59706	$hr^{-1}(wt.\%)^{-0.33293}$
k_2	0.9987	$hr^{-1}(wt.\%)^{-0.33293}$
k_3	2.3321	$hr^{-1}(wt.\%)^{-0.33293}$

5.4.Comparison Between Experimental and Predicted Results

Tables (13-15) compare the actual and model-simulated findings for the catalytic reforming process under various process conditions (using the kinetic parameters found in the literature). As can be seen from these Tables, there is a significant variance between predicted and experimental data. Such an issue was caused by the difference between the parameter and reactions' conditions, so optimization is necessary to represent the system correctly in the software. Tables (16-19) present the error between the predicted and experimental data after the optimization and substitute all the optimal parameters inside the gPROMS system mentioned above Tables (10–12). These findings showed that the fixed

bed reactor mathematical model for the catalytic reforming process can now be applied with confidence to reactor design because it was valid to very accurately simulate the fixed bed reactor's performance in the range of operation conditions studied among all concentrations with an average absolute error of less than 5%.

Table 13 Comparison Between Experimental Products and Predicted Products for Mo2C.Pt/HY Zeolite.

Reaction temperature	Reaction pressure bar	Paraffins wt.%			Naphthenes wt.%			Aromatics wt.%		
		Experimental	Predicted	Error%	Experimental	Predicted	Error%	Experimental	Predicted	Error%
480	15	63.9	54	15.492	12.72	5.12	59.748	23.38	30.98	32.506
480	12.5	64.02	59	7.841	12.08	7.18	40.562	23.9	28.8	20.502
480	10	64.76	70.1	8.245	15.34	22.04	43.676	19.9	13.2	33.668
500	15	60.3	50.9	15.588	15.3	8.48	44.575	24.4	31.22	27.950
500	12.5	62.53	55.32	11.530	13.11	3.71	71.700	24.36	33.76	38.587
500	10	63.71	68.4	7.361	12.35	23.59	91.012	23.94	12.7	46.950
520	15	62	49.5	20.161	12.17	3.98	67.296	25.83	34.02	31.707
520	12.5	62.66	57.33	8.506	14.41	6.86	52.394	22.93	30.48	32.926
520	10	60.58	66.9	**10.43	12.85	21.87	70.194	26.57	17.55	33.948

Table 14 Comparison Between Experimental Products and Predicted Products for Mo2C.Pt/Cey Zeolite.

Reaction temperature ℃	Reaction pressure Bar	Paraffins wt.%			Naphthenes wt.%			Aromatics wt.%		
		Experimental	Predicted	Error%	Experimental	Predicted	Error%	Experimental	Predicted	Error%
480	15	60.74	50.4	17.023	13.67	29.9	118.727	25.59	19.7	23.016
480	12.5	61.52	55.21	10.256	12.04	32.77	172.176	26.44	12.02	54.538
480	10	63.16	49.7	21.310	13.03	40.43	210.283	23.81	9.87	58.546
500	15	60.42	48.8	19.232	13.02	29.33	125.268	26.56	21.87	17.658
500	12.5	64.74	55.19	14.751	11.95	19.6	64.016	23.31	25.21	8.151
500	10	61.43	68.5	11.509	13.91	27.8	99.856	24.66	3.7	84.99
520	15	64.93	52.88	18.558	10.11	17.77	75.766	24.96	29.35	17.588
520	12.5	66.98	60.99	8.942	12.36	19.01	53.802	20.66	20	3.1945
520	10	61.85	69.01	11.576	13.58	22.7	67.157	24.57	8.29	66.259

Table 15 Comparison Between Experimental Products and Predicted Products for Pt.Ti/HY Zeolite.

Reaction temperature ℃	Reaction pressure bar	Paraffins wt.%			Naphthenes wt.%			Aromatics wt.%		
		Experimental	Predicted	Error%	Experimental	Predicted	Error%	Experimental	Predicted	Error%
480	15	60.4	54.98	8.97	12.2	20.38	67.049	26.4	24.64	6.667
480	12.5	60.3	49.98	17.11	13.3	19.33	45.338	25.4	30.69	20.826
480	10	60.4	52.28	13.44	13.8	30.62	121.88	25.8	17.1	33.720
500	15	61.9	50.01	19.20	11.4	17.9	57.017	26.7	32.09	20.187
500	12.5	64.5	53.22	17.48	12.1	20.03	65.53	23.4	26.75	14.3162
500	10	65.3	55.55	14.9310	11.9	15.94	33.94	22.8	28.51	25.043
520	15	63.5	52.22	17.763	9.34	19.44	108.137	27.2	28.34	4.1911
520	12.5	62.3	67.88	8.9566	12.5	18.34	46.72	25.5	13.78	45.960
520	10	64	69.109	7.982	12.3	15.54	26.341	23.7	15.351	35.227

Table 16 Simulation and Experimental Results for Mo2C.Pt/HY Zeolite.

Reaction temperature °C	Reaction pressure bar	Paraffins wt.%			Naphthene wt.%			Aromatics wt.%		
		Experimental	Predicted	Error%	Experimental	Predicted	Error%	Experimental	Predicted	Error%
480	15	63.9	62.8	1.721	12.72	13.35	4.952	23.38	22.75	2.694
480	12.5	64.02	64.5	0.749	12.08	11.85	1.90	23.9	24.13	0.962
480	10	64.76	66.04	1.976	15.34	14.92	2.737	19.9	20.32	2.110
500	15	60.3	60.9	0.995	15.3	16.06	4.967	24.4	23.64	3.114
500	12.5	62.53	63.2	1.071	13.11	12.99	0.915	24.36	24.48	0.4926
500	10	63.71	65.74	3.186	12.35	12.63	2.267	23.94	23.66	1.169
520	15	62	63.94	3.129	12.17	12.75	4.765	25.83	25.25	2.245
520	12.5	62.66	60.12	4.053	14.41	14.91	3.469	22.93	22.43	2.180
520	10	60.58	63.07	4.110	12.85	13.05	1.556	26.57	26.37	0.752

Table 17 Simulation and Experimental Results for Mo2C.Pt/Cey Zeolite.

Reaction temperature °C	Reaction pressure bar	Paraffins wt.%			Naphthene wt.%			Aromatics wt.%		
		Experimental	Predicted	Error%	Experimental	Predicted	Error%	Experimental	Predicted	Error%
480	15	63.9	61.33	0.971	12.72	14.17	3.657	23.38	24.5	4.259
480	12.5	64.02	60.41	1.804	12.08	11.88	1.328	23.9	27.71	4.803
480	10	64.76	63.83	1.060	15.34	13.46	3.300	19.9	22.71	4.619
500	15	60.3	61.91	2.466	15.3	12.77	1.920	24.4	25.32	4.668
500	12.5	62.53	63.93	1.251	13.11	11.62	2.761	24.36	24.45	4.8906
500	10	63.71	62.09	1.074	12.35	14.22	2.228	23.94	23.69	3.933
520	15	62	65.62	1.062	12.17	10.58	4.648	25.83	23.8	4.647
520	12.5	62.66	66.08	1.343	14.41	12.91	4.449	22.93	21.01	1.694
520	10	60.58	63.13	2.06	12.85	12.99	4.344	26.57	23.88	2.808

Table 18 Simulation and Experimental Results for Pt.Ti/HY Zeolite.

Reaction temperature °C	Reaction pressure bar	Paraffins wt.%			Naphthene wt.%			Aromatics wt.%		
		Experimental	Predicted	Error%	Experimental	Predicted	Error%	Experimental	Predicted	Error%
480	15	63.9	62.11	2.831	12.72	12.74	4.426	23.38	25.15	4.734
480	12.5	64.02	61.93	2.70	12.08	13.21	0.676	23.9	24.86	2.125
480	10	64.76	59.87	0.877	15.34	13.48	2.318	19.9	26.65	3.294
500	15	60.3	62.12	0.355	15.3	11.92	4.561	24.4	25.96	2.771
500	12.5	62.53	65.03	0.821	13.11	12.54	3.636	24.36	22.43	4.145
500	10	63.71	66.01	1.087	12.35	12.32	3.529	23.94	21.67	4.956
520	15	62	65.14	2.582	12.17	8.97	3.961	25.83	25.89	4.816
520	12.5	62.66	61.51	1.268	14.41	11.93	4.56	22.93	26.56	4.156
520	10	60.58	62.99	1.578	12.85	12.76	3.739	26.57	24.25	2.3206

Table.19 Simulation and Experimental Results for RON of all Catalysts.

Reaction temperature °C	Reaction pressure bar	Mo_2C.Pt/HY zeolite RON			Mo_2C.Pt/CeY zeolite RON			Pt.Ti/HY zeolite RON		
		Experimental	Predicted	Error%	Experimental	Predicted	Error%	Experimental	Predicted	Error%
480	15	73.3	76.9	4.911	73.3	76.82	4.80	81.2	84.6	4.187
480	12.5	72.8	76.33	4.848	71.4	74.823	4.7941	81	85	4.938
480	10	71.8	74.88	4.289	72.8	70.09	3.722	79	82	3.797
500	15	78.2	80.2	2.557	78.2	80.56	3.017	83.2	87	4.567
500	12.5	75.8	77.65	2.4406	70.8	73.98	4.491	82	85.3	4.024
500	10	72.8	73.74	1.2912	72.5	70.02	3.42	81.9	79.8	2.564
520	15	76.5	80.03	4.614	76.5	79.95	4.509	86.2	89.93	4.327
520	12.5	74.8	77.12	3.101	70.8	73.33	3.573	85	88	3.529
520	10	73.4	76.55	4.291	73.3	76.82	4.802	84.6	80.44	4.917

6. CONCLUSION

The present study has prepared and evaluated new composite catalysts using a heavy naphtha reformer pilot plant. The investigation results concluded that adding titanium to Pt/HY zeolite significantly improved the catalyst's ability to reform heavy naphtha. The best results of yield and RON was achieved by Pt.Ti/HY zeolite at 15 bar and 520 ℃ of 86.2. for the Mo2C.Pt/HY zeolite, the best result was at 78.2 at 15 bar and 500 ℃. The third catalyst (Mo2C.Pt/CeY zeolite) resulted in 78.2 at 500 ℃ and 15 bar. Such results are good for new catalysts used for the first time in the heavy naphtha reforming inside a pilot plant. A better design and operation of the catalytic reforming process were made possible through simulation and optimization. Constructing a trustworthy process model was necessary for significant simulation and optimization to inexpensively build alternative designs and operating scenarios. To do this, the best kinetic parameters in a fixed bed reactor used for the reforming process must be obtained. The optimal kinetic parameters of these reactions were calculated for the catalytic reforming process using an optimization approach that depends on the reduction of summation of square errors (SSE) between the model-predicted yield and experimental yield and RON with nonlinear (NLN) regression. With an average absolute error of less than 5% across all results at various operating conditions, nonlinear regression was used to determine the kinetic parameters, which was proved to be more accurate and showed excellent agreement with the experimental results, which unequivocally demonstrates that the models (in addition to forecasting the concentration profiles of every component at any circumstance) can be effectively used for reactor design.

NOMENCLATURE

Symbol	Meaning	Unit
$\Delta\rho_P$	Pressure dependence of liquid density	lb/ft^3
$\Delta\rho_P$	Temperature correction of liquid density	lb/ft^3
C_{in}	Initial concentration (inlet to reactor)	cm^3/mol
C_{out}	Final concentration (outlet from reactor)	cm3/mol
D_{Ki}	Knudsen diffusivity factor	cm^2/s
D_{ei}	Effective diffusivity	cm^2/s
D_{mi}	Molecular diffusivity	cm^2/s
d_p	Particle diameter	cm
d_t	Tube diameter	cm
K_o	Frequency or pre-exponential factor	cm^3/g·s
K_{app}	Apparent reaction rate constant	(time)$^{-1}$(concentration)$^{1-n}$
K_{in}	Kinetic rate constant	(time)$^{-1}$ (concentration)$^{1-n}$
MW_i	Molecular weight of oxygen,	g/g mol
Mw_L	Molecular weight of liquid phase	g/g mol
r_g,	Mean pore radius	cm
r_p	Radius of particle	cm
S_g	Specific surface area of particle	cm^2/g
SP	External surface area of catalyst particle	cm^2
sp $gr_{15.6}$	Specific gravity of oil at 15.6 °C	-
T_{meABP}	Mean average boiling point	R
u_L	Velocity of the liquid	cm/s
V_{CL}	Critical specific volume of liquid	cm^3/mol
V_g	Total pore volume	cm^3/g
V_L	Molar volume of liquid at its n.b. temperature	cm^3/mol
V_P	Volume of catalyst particle	cm^3
μ_L	Dynamic viscosity of liquid phase	mPa·s
$\rho_{15.6}$	Density of light gas oil at 15.6 °C	g/cm^3
ρ_B	Bulk density	g/cm^3
ρ_L	Liquid density at process condition	lb/ft^3
ρ_{HN}	Density of heavy naphtha at 15.6 °C and 101.3 kPa	lb/ft^3
ρ_p	Particle density	g/cm^3
a	Dimensionless number	-
EA	Activation energy	kJ/mol
G	Acceleration	cm/s^2
K	Reaction rate constant	h^{-1}*wt$^{(n-1)}$
N	Order of reaction kinetic	-
R	Universal gas constant	8.314 J/mol·K
T	Temperature	K or °C
V	Bed volume of particle catalyst	cm^3
V_P	Pore volume	cm^3
V_L	Volumetric flow of liquid phase	cm^3/time
$\mathcal{T}$	the tortuosity factor	-

ACKNOWLEDGEMENTS

The authors are grateful for the financial support towards this research by the Chemical Engineering Department, College of Engineering, Tikrit University. Postgraduate Research Grant (PGRG) No.TU.G/2021/HIR/MOHE/ENG/39 (2895-7-3).

REFERENCES

[1] Ahmedzeki NS, Al-Tabbakh BA. **Catalytic Reforming of Iraqi Naphtha Over Pt-Ti/HY Zeolite Catalyst**. *Iraqi Journal of Chemical and Petroleum Engineering* 2016; **17**(3): 45–56.

[2] Al-Taaie AK, Mohammad WS, Jubear AJ. **Numerical Simulation of the Collector Angle Effect on the Performance of the Solar Chimney Power Plant**. *Al-Khwarizmi Engineering Journal* 2016; **12**(2): 79–89.

[3] Baraket L, Ghorbel A, Grange P. **Selective Catalytic Reduction of no by Ammonia on V2O5–SO42−/Tio2 Catalysts Prepared by the Sol–Gel**

Method. *Applied Catalysis B: Environmental* 2007; **72**(1–2): 37–43.

[4] Rahimpour MR, Jafari M, Iranshahi D. **Progress in Catalytic Naphtha Reforming Process: A Review**. *Applied Energy* 2013; **109**:79–93.

[5] Lee S. *Encyclopedia of Chemical Processing* 2006; **1**: Taylor & Francis US.

[6] Parker JE, Gomez-Gonzalez M, Van Lishout Y, Islam H, Duran Martin D, Ozkaya D, Quinn PD, Schuster ME, **a Cell Design for Correlative Hard X-Ray Nanoprobe and Electron Microscopy Studies of Catalysts Under in Situ Conditions**. *Journal Synchrotron Radiat* 2022; **29**:2.

[7] Lin Z, Ammal S.C, Denny S.R, Rykov S.A, You K.E, Heyden A, Chen J.G. **Unraveling Unique Surface Chemistry of Transition Metal Nitrides in Controlling Selective C–O Bond Scission Pathways of Glycerol**. *JACS Au* 2022; **2**(2): 367–379.

[8] Hodala J.L, Kotni S, Chelliahn B. **Metal Carbide as a Potential non Noble Metal Catalyst for Naphtha Reforming**. *Fuel* 2021; **288**: 119610.

[9] S. Sarıkoç. **Fuels of the Diesel-Gasoline Engines and Their Properties**. *Diesel and Gasoline Engines* 2020; **31**.

[10] Calvin YL, Hariyanto PAT, Usman AI, Masuku M, Wibowo CS, Anggarani, R, Sugiarto B. **Volatility and Physicochemical Properties of Gasoline-Ethanol Blends with Gasoline RON-Based 88, 90, and 92**. *Fuel* 2022; **307**: 121850.

[11] Tregubenko VY, Vinichenko NV, Talzi VP, Belyi AS. **Catalytic Properties of the Platinum Catalyst Supported on Alumina Modified by Oxalic Acid in N-Heptane Reforming**. *Russian Chemical Bulletin*, 2020; **69**: 1719–1723.

[12] Shan P, Niu P, Zhang H, Zhang H, Lu N, Wang Y, Fan B, Li R. **SSZ-13 Supported Ir as an Efficient Catalyst for Methylcyclopentane Ring-Opening Reaction**. *Catalysis Communications* 2021; **154**: 106311.

[13] Ahmedzeki NS, Al-Tabbakh BA, Antwan MB, Yilmaz S. **Heavy Naphtha Upgrading by Catalytic Reforming Over Novel Bi-Functional Zeolite Catalyst**. *Reaction Kinetics, Mechanisms and Catalysis* 2018; **125**: 1127–1138.

[14] Fatimah S, Ragadhita R, Al Husaeni DF, Nandiyanto ABD. **how to Calculate Crystallite Size from X-Ray Diffraction (XRD) Using Scherrer Method**. *ASEAN Journal of Science and Engineering* 2022; **2**(1): 65–76.

[15] Lin C, Pan H, Yang Z, Han X, Tian P, Li P, Xiao Z, Xu J, Han YF. **Effects of Cerium Doping on Pt–Sn/Al2O3 Catalysts for N-Heptane Reforming**. *Industrial & Engineering Chemistry Research* 2020; **59**(14): 6424–6434.

[16] Verma V, Mishra A, Anand M, Farooqui SA, Sinha AK. **Catalytic Hydrocracking of Inedible Palm Stearin for the Production of Drop-In Aviation Fuel and Comparison with Other Inedible Oils**. *Renewable Energy* 2022; **199**:1440–1450.

[17] Tang Y, Luo G, Zhong J, Chen K, Xu C, Cheng Z**. Effects of Stagnant Zone on the Effectiveness Factor in a Trickle Bed**. *Chemical Engineering Science* 2022; **248**:117211.

[18] Mederos FS, Elizalde I, Ancheyta J. **Steady-State and Dynamic Reactor Models for Hydrotreatment of Oil Fractions: A Review**. *Catalysis Reviews* 2009; **51**(4):485–607.

[19] Jarullah AT, Mujtaba IM, Wood AS. **Improving Fuel Quality by Whole Crude Oil Hydrotreating: a Kinetic Model for Hydrodeasphaltenization in a Trickle Bed Reactor**. *Applied Energy* 2012; **94**: 182–191.

[20] Etemadi O, Yen TF. **Aspects of Selective Adsorption Among Oxidized Sulfur Compounds in Fossil Fuels**. *Energy & Fuels* 2007;**21**(3):1622–1627.

[21] Devatha CP, Vishnu Vishal A, **Purna Chandra Rao J. Investigation of Physical and Chemical Characteristics on Soil Due to Crude Oil Contamination and its Remediation**, *Applied Water Science* 2019; **9**: 1–10.

[22] Šašić S, Veriotti T, Kotecki T, Austin S. **Comparing the Predictions by NIR Spectroscopy Based Multivariate Models for Distillation Fractions of Crude Oils by F-Test**. *Spectrochimica Acta Part A: Molecular and Biomolecular Spectroscopy* 2023; **286**: 122023.

[23] Hasan ZW, Hasan ZW, Sultan AJ, Sabri LS, Ali JM, Salih HG, Majdi HS, Al-Dahhan MH. **Experimental Investigation on the Impact of Tube Bundle Designs on Heat Transfer Coefficient in Gas-Solid Fluidized Bed Reactor for Fischer-Tropsch Synthesis**. *International Communications in Heat and Mass Transfer* 2022; **136**:106169.

[24] Jarullah AT, Mujtaba IM, Wood AS. **Kinetic Model Development and Simulation of Simultaneous Hydrodenitrogenation and Hydrodemetallization of Crude Oil in Trickle Bed Reactor**. *Fuel* 2011: **90**(6): 2165–2181.

[25] Jiménez F, Kafarov V, Nunez M. **Modeling of Industrial Reactor for Hydrotreating of Vacuum Gas Oils: Simultaneous Hydrodesulfurizatio n, Hydrodenitrogenation, and Hydrodearomatization Reactions**. *Chemical Engineering Journal* 2007; **134**(1–3):200–208.

[26] Jarullah AT, Ahmed AM, Hussein HM, Ahmed AN, Mohammed HJ. **Evaluation of Synthesized Pt/HY-H- Mordenite Composite Catalyst for Isomerization of Light Naphtha**. *Tikrit Journal of Engineering Sciences* 2023; **30**(1–3):94–103.

[27] Hamadi AS. **Selective Additives for Improvement of Gasoline Octane Number**. *Tikrit Journal of Engineering Sciences* 2010; **17**(2): 22–35.

[28] Ibrahim MM, A'reff HA, Jarallah AT. **Kinetic Models Study of Hydrogenation of Aromatic Hydrocarbons in Vacuum Gas Oil and Basrah Crude Oil Reaction**. *Tikrit Journal of Engineering Sciences* 2009; **16**(4): 1–11.